POPX2 phosphatase regulates the KIF3 kinesin motor complex

Phang, Hui-Qun; Hoon, Jing-Ling; Lai, Soak-Kuan; Zeng, Yukai; Chiam, Keng-Hwee; Li, Hoi-Yeung; Koh, Cheng-Gee

2014

Phang, H.-Q., Hoon, J.-L., Lai, S.-K., Zeng, Y., Chiam, K.-H., Li, H.-Y., et al. (2014). POPX2 phosphatase regulates the KIF3 kinesin motor complex. Journal of cell science, 127(4), 727-739.

https://hdl.handle.net/10356/106722

https://doi.org/10.1242/jcs.126482

POPX2 Phosphatase Regulates the KIF3 Kinesin Motor Complex

Hui-Qun Phang[1,§], Jing-Ling Hoon[1,§], Soak Kuan Lai[1,§], Yukai Zeng[2], Keng-Hwee Chiam[2,3], Hoi Yeung Li[1], and Cheng-Gee Koh[1, 3, *]

[1]School of Biological Sciences, College of Science, Nanyang Technological University, Singapore 637551
[2]Bioinformatics Institute, ASTAR, Singapore 138671
[3]The Mechanobiology Institute, Singapore 117411

[§]These authors contributed equally to this work.

* Author for correspondence (cgkoh@ntu.edu.sg)

Running title: Phosphorylation regulates KIF3A

SUMMARY

The kinesin motors are important in the regulation of cellular functions such as protein trafficking, spindle organization and centrosome separation. In this study, we have identified POPX2, a serine-threonine phosphatase, as an interacting partner of the KAP3 subunit of the kinesin-2 motor. The kinesin-2 motor is a heterotrimeric complex composed of KIF3A, KIF3B motor subunits and KAP3, the non-motor subunit, which binds the cargo. Here we report that the phosphatase POPX2 is a negative regulator of the trafficking of N-cadherin and other cargoes; consequently, it markedly influences cell-cell adhesion. POPX2 affects trafficking by determining the phosphorylation status of KIF3A at serine-690. This is consistent with the observation that KIF3A-S690A mutant is defective in cargo trafficking. Our studies also implicate CaMKII as the kinase that phosphorylates KIF3A at serine-690. These results strongly suggest POPX2 and CaMKII as the phosphatase-kinase pair that regulates kinesin-mediated transport and cell-cell adhesion.

Keyword: Calcium-calmodulin kinase, Kinesin-2 motor, N-cadherin, POPX2 phosphatase

INTRODUCTION

The kinesin motors have diverse functions in eukaryotic cells. They are responsible for the transport and trafficking of vesicles, organelles and proteins along the microtubule network as well as for the separation of the centrosomes and the organization of the mitotic spindles during cell division. Thus far about 14 kinesin families and some orphan kinesins have been identified. Most of the kinesins are plus end motors but some e.g. kinesin-14 are reported to be minus end motors (Endow et al., 2010). The activities of the kinesin motors in the cell are regulated to ensure that cargoes are directed to the right place at the right time. The KIF3 motor belongs to the kinesin-2 family. It is a heterotrimeric motor, which comprises the KIF3A and KIF3B motor subunits and a non-motor KAP3 (KIF-associated protein 3) subunit (Hirokawa, 2000). KAP3 contains armadillo repeats, which are thought to mediate protein-protein interaction and regulate binding with the cargo proteins. To date, N-cadherin, adenomatous polyposis coli (APC), β-catenin, fodrin and Rab11-containing vesicles have been identified as cargoes transported by the KIF3 motor (Takeda et al., 2000; Jimbo et al., 2002; Teng et al., 2005; Schonteich et al., 2008; Hirokawa et al., 2009).

The POPX (partner of PIX) phosphatases belong to the PP2C serine-threonine phosphatase family. So far, two members, POPX1 and POPX2, have been identified (Koh et al., 2002). The larger POPX1 is found predominantly in the brain and testis whereas POPX2 is ubiquitous. The main substrates of POPX2 identified thus far are the p21-activated kinase (PAK) and calcium calmodulin kinases (CaMK) (Ishida et al., 1998; Koh et al., 2002). POPX2 is found in a complex with PIX (PAK interacting exchange factor), which is a guanine nucleotide exchange factor for RAC1 and CDC42 (Koh et al., 2002). The SH3 domain of PIX, on the other hand, binds strongly to PAK (Manser et al., 1998), suggesting that POPX2 is in close proximity of an activator (PIX) and effector (PAK) of the Rho GTPases. POPX2 has also been shown to interact with the formin protein mDia1 and can regulate mDia1 and RhoA regulated transcription mediated by serum response factor (Xie et al., 2008). The levels of POPX2 are found to be higher in invasive cancer (Susila et al., 2010). Overexpression of POPX2 also results in higher cell motility, which suggests that POPX2 may regulate proteins other than PAK and CaMK. One other pathway

regulated by POPX2 is the Glycogen Synthase Kinase 3 (GSK3) pathway (Singh et al., 2011; Zhang et al., 2013). However, GSK3 is not a direct substrate of POPX2.

In an attempt to understand more about the physiological roles of POPX2 and the biochemical pathways that POPX2 regulates, a yeast two-hybrid screen was conducted to identify POPX2 interaction proteins. KAP3, a subunit of the KIF3 motor, was identified as an interacting partner of POPX2. Investigating the physiological significance of this interaction, we find that fibroblasts overexpressing POPX2 are impaired in KIF3 motor-mediated transport of N-cadherin to the cell periphery and are, consequently, defective in cell-cell adhesion. The transport of other KIF3 motor cargoes such as the Rab11-containing vesicles, is also similarly affected by POPX2 in a phosphatase activity-dependent manner. Our findings suggest that POPX2 determines the phosphorylation status of the KIF3 kinesin motor and, in turn, regulates cell-cell adhesion.

RESULTS

POPX2 interacts with the KIF3 motor complex

KAP3, the non-motor subunit of the KIF3 motor complex, was found to be an interacting partner of POPX2 in a yeast two-hybrid screen. To confirm this interaction by immunoprecipitation, we used GFP-tagged human POPX2 cDNA to generate stable NIH3T3 fibroblast cell line since no antibodies are available to detect mouse POPX2. We found that the endogenous KAP3 co-immunoprecipitated with GFP-POPX2 (Fig. 1A). KAP3 also interacted with POPX1. Using deletion analysis, we mapped the KAP3 interacting region near the N-terminal of both POPX1 (residue 236 to 269) and POPX2 (residue 150 to 193) (Fig. 1B, C). This region of POPX also overlaps with the region responsible for POPX's interaction with PIX (Koh et al., 2002). As PIX, POPX2 and KAP3 can form a trimeric complex (Fig. S1A), this suggests that PIX and KAP3 interact with POPX2 at different sites. Meanwhile, we also tested if POPX2 might interact with KIF3A and KIF3B. This is because a dual specificity phosphatase Dusp26 has been reported to interact with both KIF3A and KAP3 (Tanuma et al., 2009). We found that both KAP3 and KIF3A co-immunoprecipitated well with POPX2 (Fig. S1B). However, little KIF3B was found in the POPX2 pulldown. The armadillo repeats on KAP3 are responsible for

interacting with POPX2. There are three clusters of armadillo repeats on the KAP3 protein. Both clusters 1 and 3 showed binding to POXP2 (Fig. 1D).

N-Cadherin localization to the cell periphery is affected by POPX2

In order to determine the possible roles of POPX2-KAP3 interaction, we investigated if the transport of the KIF3 cargoes is affected by POPX2. Since N-cadherin has been reported to be a cargo of the KIF3 motor and is normally localized to the cell periphery (Teng et al., 2005), we decided to study its localization in control NIH3T3 cells and stable POPX2-overexpressing cell line (X2). N-cadherin failed to localize to the cell periphery in POPX2 overexpressing cells (Fig. 2A). Similarly another reported cargo of the KIF3 motor, β-catenin (Teng et al., 2005), also mislocalized in POPX2 overexpressing cells. β-catenin no longer localized to the cell-cell junctions in POPX2 overexpressing cells (Fig. 2B). The levels of N-cadherin and β-catenin were not affected by the overexpression of POPX2 (Fig. 2C). However, the amount of N-cadherin found at the cell surface is much reduced in cells overexpressing POPX2 (Fig. 2D). It is unlikely that the presence of POPX2 affected the interaction between KAP3 and N-cadherin as similar amounts of KAP3 and N-cadherin were co-immunoprecipitated in both the control cells and POPX2 overexpressing cells (Fig. 2E). The presence of POPX2 also did not affect the interaction between KIF3A and KAP3 (Fig. 2F). These observations imply that POPX2 might affect the transport of the KIF3 cargoes to their destinations in the cells.

We next investigated if the phosphatase activity of POPX2 was required to perturb the transport of KIF3 cargo. NIH3T3 cells were transfected with GFP-POPX2 and a phosphatase dead mutant, GFP-POPX2m (Koh et al., 2002). We found that localization of N-cadherin and β-catenin was affected by POPX2 but not POPX2m, suggesting that the phosphatase activity of POPX2 was responsible for the impairment of KIF3 motor-mediated transport (Fig. 3A, B).

POPX2 overexpressing cells show defective cell-cell adhesion

N-cadherin is one of the major components of the adherens junctions in NIH3T3 cells. Since POPX2 overexpressing cells showed impaired N-cadherin localization, we determined if cell-cell adhesion was also affected. Briefly, cells were suspended

with and without calcium or EGTA (ethylene glycol tetraacetic acid) for a fixed time interval. The number of aggregates formed was then counted. As cadherins require calcium to mediate cell-cell interaction, incubation of the cells without calcium or with EGTA to chelate the calcium ions would result in loss of cell aggregation. Similarly if N-cadherin were not properly localized to the cell periphery, no cell aggregation would occur. As expected, POPX2 expressing cells did not form aggregates in the presence of 2mM $CaCl_2$. However, aggregation among the control cells as well as the POPX2m expressing cells was not affected (Fig. 3C). In the presence of POPX2, the efficiency of cell aggregation mediated by calcium was reduced to about 30% compared to that by control cells (Fig. 3D). Thus, the aggregation assay strongly correlates POPX2-mediated inhibition of N-cadherin localization to the cell periphery with the loss of cell-cell adhesion.

Transport by the KIF3 motor is affected by POPX2

We next tracked the transport of a KIF3 cargo, N-cadherin using live cell imaging. NIH3T3 cells were doubly transfected with N-cadherin-GFP and mCherry-POPX2 or mCherry-POPX2m cDNA constructs. The trafficking of N-cadherin-GFP was monitored. The movement of N-cadherin-GFP was retarded in POPX2 expressing cells but not in POPX2m expressing cells or the control cells transfected with mCherry vector construct (Fig. 4A and Supplementary Movie 1). The mean velocity exhibited by these N-cadherin-GFP vesicles suggests that POPX2 severely affects the trafficking of N-cadherin (Fig. 4B).

To determine if the defects we observed were due to the impairment of KIF3 motor mediated transport, we included two other control experiments. HeLa cells were used to show that the phenomenon we observed is not cell type specific but due to the influence of POPX2 on the KIF3 motor. As Rab11-containing vesicles are also transported by the KIF3 motor (Schonteich et al., 2008), we monitored the trafficking of dsRed-Rab11 in GFP-POPX2 and GFP-POPX2m expressing cells. Similar to what was observed for N-cadherin, the trafficking of Rab11-containing vesicles was impaired in the presence of POPX2 but not POPX2m (Fig. 4C, D; Supplementary Movie 2). In addition, POPX2 also caused the clustering of Rab11-containing vesicles (Fig. 4E, F). However, the trafficking of clathrin light chain A-containing vesicles, which was not a cargo of the KIF3 motor, was not affected by POPX2 (Fig. 4G, H;

Supplementary Movie 3). We have also included an additional control experiment to show that overexpression of POPX2 does not affect the trafficking of mitochondria (Fig. 4I), suggesting that POPX2 specifically affects cargoes transported by the KIF3 motor. Immunostaining using α-tubulin antibodies also suggests that POPX2 does not cause observable defects to the microtubule network (Fig. S2A). We have also confirmed that N-cadherin-GFP is localized to early endosomes and secretory vesicles by co-staining with EEA1 and chromogranin A, respectively (Fig. S2B). This is consistent with earlier reports of N-cadherin localization to the plasma membrane, Golgi, endocytic and secretary vesicles (Mary et al., 2002). Kinesin-2 has been detected in cell fractions containing both early and late endocytic vesicles, and addition of antibodies targeting kinesin-2 resulted in decreased directional movement of endosomes (Loubery et al., 2008).

Serine-690 of KIF3A is important in the regulation of KIF3 motor transport

Having found that the POPX2 phosphatase profoundly affects the trafficking of KIF3 cargoes we proceeded to determine the underlying mechanism. We hypothesized that POPX2 regulates the KIF3 motor through the control of KIF3 phosphorylation status. Our observations thus far suggest that dephosphorylated KIF3 motor complex is impaired in cargo transport.

Various phosphoproteomic-based analysis have identified the serine-690 residue on the C-terminal tail of KIF3A as a major phosphorylation site (Ballif et al., 2004; Dephoure et al., 2008; Pan et al., 2008; Tweedie-Cullen et al., 2009; Huttlin et al., 2010; Olsen et al., 2010; Wisniewski et al., 2010). This serine residue falls within the putative consensus sequence R-X-X-S for CaMKII and this sequence is found to be conserved among human, mouse and zebrafish KIF3A (Fig. 5A). Hence, we generated KIF3A-S690 mutants and monitored their effects on KIF3 cargo transport. Serine-690 was mutated to alanine (S690A) to preclude phosphorylation, or to aspartic acid (S690D) to mimic constitutive phosphorylation.

We first determined the consequence of mutating KIF3A-S690 on the distribution of N-cadherin. Stable cell lines overexpressing GFP-KIF3A-WT, GFP-KIF3A-S690A or GFP-KIF3A-S690D, were generated by retroviral infection of the NIH3T3 cells. Immunofluorescence staining of the endogenous N-cadherin showed that overexpression

of the KIF3A-S690A mutant led to a decreased localization of N-cadherin to the cell periphery and cell-cell junctions (Fig. 5B). We also observed that overexpression of KIF3A-S690A, but not KIF3A-WT and KIF3A-S690D, led to less N-cadherin at the cell surface (Fig. 5C). We then examined the effect of mutating KIF3A-S690 on the motility of N-cadherin-GFP. Long centrifugal movement of N-cadherin-GFP was observed in NIH3T3 cells overexpressing mCherry-KIF3A or mCherry-S690D mutant, indicating that overexpression of these proteins did not cause significant changes in the motility of N-cadherin vesicles (Fig. 5D and Supplementary Movie 4). However, movement of N-cadherin-GFP was impaired in cells overexpressing the mCherry-S690A mutant (Fig. 5D and Supplementary Movie 4). We have noticed that this impairment occurred only in cells with very high expression of mCherry-S690A. Cells with low or moderate expression of mCherry-S690A did not show significant changes in the motility of the N-cadherin vesicles. This might be due to the basal activity of endogenous wild type KIF3A. On the other hand, high expression of mCherry-KIF3A and mCherry-S690D did not have any apparent effect on the N-cadherin transport, indicating that the inhibition on N-cadherin trafficking in mCherry-S690A overexpressing cells was not due to off-target effects caused by high levels of protein expression. Calculation of mean velocity showed that the KIF3A-S690A mutant affected trafficking of N-cadherin (Fig. 5E).

Next, we determined if overexpression of the KIF3A-S690A mutant perturbs the motility of Rab11. Again, using live cell imaging, we observed that the dsRed-Rab11 vesicles were less motile and accumulated more around the perinuclear region in cells that overexpressed GFP-KIF3A-S690A (Fig. 5F and Supplementary Movie 5). The KIF3A-S690A mutant also affected the mean velocity of Rab11-containing vesicles (Fig. 5G). The KIF3A-S690D mutant did not affect the trafficking of Rab11-containing vesicles. Taken together, our results suggest that the phosphorylation status of the KIF3A serine-690 residue is crucial in regulating cargo transport.

In order to remove biasness in manual tracking of N-cadherin or Rab11 vesicles, we have used particle segmentation and tracking algorithms to track every fluorescent particle in the cells in all our analyses. Representative tracks in control and X2 cells are shown in Figure S3 (Fig. S3A, B). In addition, we have also found that the average velocity of N-cadherin trafficking ranges from ~0.2 to 0.36 μm/s depending on the cell type. Additional experiments were also conducted at different frame rates

for the live imaging. We did not observe any differences arising from different frame rates used (1 frame/3s versus 2 frames/s, Fig S3C).

Phosphorylation of KIF3A-S690 does not affect cargo binding affinity

Previous studies have reported that phosphorylation of serine residues in the C-terminal tail of kinesin motor modulates the affinity of cargo binding (Ichimura et al., 2002; Guillaud et al., 2008; Vagnoni et al., 2011). Thus, we sought to elucidate if mutation of serine-690 of KIF3A affects binding of molecular cargo. Since N-cadherin associates with the KIF3 motor primarily through the KAP3 subunit, we determined if the binding between KAP3 and the various KIF3A mutants is affected. GST-KAP3 was co-expressed with various FLAG-tagged KIF3A constructs and the cell lysates were subjected to FLAG immunoprecipitation. Wild type KIF3A, KIF3A-S690A and KIF3A-S690D interacted equally well with GST-KAP3 in these assays and no interaction was observed between FLAG-KIF3A and the control, GST (Fig. 6A). The lack of effect of mutating KIF3A serine-690 on KAP3 binding implies that the inhibition on cargo transport is not due to modulation of binding affinity between KIF3A and KAP3.

We also checked if the interaction between the motor domain and the tail domain of KIF3A is affected by S690 phosphorylation. GST-tagged tail domain (aa 601 to 702) constructs of KIF3A-WT, KIF3A-S690A and KIF3A-S690D were tested for their interaction with the motor domain (aa 1 to 354). We found that all three tail domain constructs bound similarly well with the motor domain, suggesting that S690 mutation to A or D does not affect head to tail interaction of KIF3A (Fig. 6B). However, it is possible that S690 phosphorylation status may affect KIF3 motor interaction with microtubules. Therefore we immunoprecipitated KIF3A-WT, KIF3A-S690A and KIF3A-S690D from transfected HeLa cells, and determined their ability to bind to microtubules. We found that KIF3A-S690A showed weaker interaction with microtubules (Fig. 6C).

CaMKII and POPX2 regulate KIF3A-S690 phosphorylation status

Since we have established that the phosphorylation status of S690 of KIF3A is important in the transport activity of the KIF3 motor, we tested the possibility that

POPX2 directly dephosphorylates KIF3A. It is first necessary to ascertain that KIF3A-S690 is phosphorylated by CaMKII. KIF3A tail domain could indeed be phosphorylated by CaMKII in an *in vitro* kinase assay (Fig. 6D, lane 3). The S690 residue is likely to be the major phosphorylation site within the tail domain as no observable phosphorylated band was detected for the KIF3A-S690A tail domain in the presence of active CaMKII (Fig. 6D, lane 4). CaMKII could be the specific kinase that phosphorylates the KIF3A tail domain as the active PAK did not phosphorylate the KIF3A tail (Fig. 6D, lane 1). In addition, trafficking of N-cadherin-GFP is impaired in the presence of the CaMKII inhibitors (KN-93, KN-62 and AIP), suggesting that CaMKII phosphorylation may regulate the KIF3 motor complex (Fig. 7A, B, C, D, Supplementary Movie 6).

Phosphorylated KIF3A-S690 could be effectively dephosphorylated by POPX2 (Fig. 7E, lane 3). The control phosphatase, calf-intestinal phosphatase, only showed a much lesser extent of dephosphorylation when used at a higher concentration (Fig. 7E, lane 4). In the phosphatase assays using GST-tagged phosphatases pulled down from transfected cell lysates, POPX2 showed higher efficiency compared with PP2Cα and PP1 towards phosphorylated KIF3A-S690 (Fig. 7F, see Fig. S2C for purity of GST tagged phosphatases).

Silencing endogenous POPX2 does not aversely affect the KIF3 motor

Silencing endogenous POPX2 using siRNA did not lead to an increase in N-cadherin trafficking (Fig. 8). N-cadherin distribution to the cell-cell junctions (Fig. 8A) and the trafficking or motility of N-cadherin appeared to be similar in the control and POPX2 knockdown cells (Fig. 8B, C). Since the antibody against POPX2 cannot detect mouse POPX2, we have used RT-PCR to check the siRNA knockdown efficiency (Fig. 8D). As an additional control, we have also confirmed that silencing of POPX2 in HeLa cells does not affect the localization of N-cadherin to the cell periphery and motility of N-cadherin-GFP (Fig. S4). These observations are consistent with the overexpression of KIF3A-S690D (Fig. 5E, G). On the other hand, inhibition of CaMKII phosphorylation of KIF3A resulted in impairment of cargo transport. Taken together, our data suggest that under-phosphorylation of KIF3A-S690 will lead to impairment of cargo trafficking. Since we are tracking the motility of N-cadherin and

other KIF3 cargoes, it is implicit that only the phosphorylated KIF3 motor will move along the microtubules. Interestingly, overexpression of KIF3A-S690D can rescue the N-cadherin and β-catenin localization defects induced by POPX2 (Fig. S5). This observation furthers support that the phosphorylation status of S690 is important in the regulation of KIF3 motor transport.

DISCUSSION

The mechanisms by which kinesins transport their molecular cargoes to specific subcellular locations and how this transport is regulated are not clearly understood. Several modes of regulation have been suggested. In general, one mode of regulation involves modulation of the binding of kinesins to the microtubule tracks. One example of this is kinesin-1, whose phosphorylation in the motor domain (serine-176) reduces its ability to bind microtubules and to transport cargo (Morfini et al., 2009). A second mode of control involves the regulation of cargo-motor association. Phosphorylation of residues in the C-terminal tail region of kinesins has been shown to either promote or inhibit cargo binding. For instance, phosphorylation of kinesin light chain 2 on serine-575 stimulates binding of 14-3-3 cargo protein (Ichimura et al., 2002), whereas phosphorylation of KIF17 on serine-1029 disrupts the binding of Mint1 to the tail domain of the motor (Guillaud et al., 2008). Finally, a fundamental control of kinesin function comes from auto-inhibition. Soluble kinesins have been shown to assume a folded, inactive conformation, where the C-terminal region interacts with the motor domain, leading to the inhibition of the ATPase activity and the ability to bind microtubules (Friedman and Vale, 1999; Stock et al., 1999). This interaction is thought to be relieved by high ionic strength or binding of molecular cargoes, which generates an extended, active conformation. Nonetheless, cargo binding may not be the complete answer to motor activation. Kinesin-1 motors that are attached to membrane cargo can still be inactive (Wozniak and Allan, 2006). Instead, phosphorylation has been shown to play an important role in relieving kinesin auto-inhibition. It has been reported that phosphorylation of threonine-937 of KIF11 (Eg5) in the inhibitory C-terminal tail increases the efficiency of microtubule binding (Cahu et al., 2008). In a second example, phosphorylation of the inhibitory C-terminal tail of Kinesin-7 causes the motor to unfold and acquire higher processivity along the microtubules (Espeut et al., 2008).

In the current study, we have demonstrated that preclusion of phosphorylation on KIF3A serine-690 leads to impairment of cargo transport. Since serine-690 resides at the C-terminal tail domain and the KIF3 complex has been reported to adopt a folded conformation (Wedaman et al., 1996), our data suggest that phosphorylation of KIF3A on serine-690 may be important for relieving auto-inhibition. Consequently, when phosphorylation of this site is inhibited in the KIF3A-S690A mutant, we observed a reduction in cargo trafficking (Fig. 5). We hypothesize that the KIF3 motor is auto-inhibited when S690 is not phosphorylated. The auto-inhibited confirmation could be similar to other kinesin motors i.e. due to a head-to-tail interaction. The motor domain of KIF3A can still interact with the S690D C-terminal tail (Fig. 6B). However, we do not think that this observation contradicts our hypothesis that phosphorylation relieves auto-inhibition of the kinesin. It is likely that the S690D mutation may not represent a true phospho-mimic as substitution of S to D only resulted in increased positive charge. This model could be tested by the determination of the structure of the head domain in complex with the C-terminal tail domain, which contains WT, S690A or S690D. It appears that the phosphorylation status of KIF3A-S690 might affect the KIF3 motor's binding to the microtubules (Fig. 6C). This is consistent with observations of another kinesin-2 motor KIF17, which adopts a folded conformation whereby the C-terminal tail domain interacts with the motor domain and prevents the motor from binding to the microtubules (Hammond et al., 2010). Future experiments would involve further characterization of the binding of KIF3 motor to the microtubules and determining if the ATPase activity of the motor is also regulated by phosphorylation.

One remarkable feature of the KIF3 kinesin that distinguishes it from other kinesins is the presence of two different motor subunits, KIF3A and KIF3B. The physiological significance of having two different motor subunits is still unclear. Phosphoproteomic analysis has indicated that the mouse KIF3B is phosphorylated on serine-181 and serine-681 (Huttlin et al., 2010; Wisniewski et al., 2010). Serine-181 is located in the motor domain while serine-681 resides at the tail domain. Whether POPX2 regulates phosphorylation of these two sites is not known. In addition, the consensus sequence for CaMKII is not found within these sites. However, it is possible that phosphorylation of both KIF3A and KIF3B is required for full activation of KIF3

motor activity. Likewise, inhibition of merely one phosphorylation site might not totally abrogate the motor function. This may partly explain why the KIF3A-S690A mutant is able to reduce but not fully inhibit KIF3-mediated protein transport.

Our results clearly suggest the involvement of both kinase and phosphatase in the regulation of kinesin function. We have shown that KIF3A-S690 can be phosphorylated directly by CaMKII and that phosphorylation at this site may be one of the mechanisms for relieving the auto-inhibition of the KIF3 motor. Moreover, the trafficking of N-cadherin cargo is impaired in the presence of CaMKII inhibitors, suggesting the importance of CaMKII phosphorylation in KIF3-motor mediated transport (Fig. 7A to D). Dephosphorylation of KIF3A by POPX2, either directly or indirectly via the inhibition of CaMKII, on the other hand, confines the motor in an auto-inhibited state. That CaMKII is involved in the regulation of KIF3 motors also raises the possibility that calcium signaling may fine tune cargo trafficking by the kinesin motors. It is well documented that extra-cellular calcium regulates cell-cell adhesion via the cadherins. Intra-cellular calcium can also affect N-cadherin and related signaling. The influx of calcium into cells upon injury or NMDA receptor activation is known to lead to the activation of calpain, a protease sensitive to calcium. Activated calpain then cleaves N-cadherin (Jang et al., 2009). The cleavage of N-cadherin further affects cell-cell adhesion, AKT signaling, as well as N-cadherin and β-catenin interaction. However, it has also been reported that upon brain injury, astrocytes increase intracellular calcium levels, which subsequently lead to up-regulation of N-cadherin translation. Up-regulation of N-cadherin in turn plays important roles in reactive astrogliosis and neuroprotection (Kanemaru et al., 2013). In this study, we report a new mechanism that controls the amount of surface N-cadherin via the regulation of the KIF3 motor trafficking by CaMKII. Since N-cadherin is not the only cargo transported by the KIF3 motor, we expect that the localization of other KIF3 cargoes such as β-catenin, adenomatous polyposis coli protein and cell polarity proteins (Hirokawa et al., 2009) will also be similarly affected by the calcium content in the cell and the activity of CaMKII. Hence, it is not unexpected that CaMKII and POPX2 might also regulate cell polarity, particularly in neuronal cell types.

The KIF3 motor complex is also linked to tumour suppression. Conditioned knockout of KAP3 in mouse embryos leads to tumour-like growth in the brain (Teng et al., 2005). This has been attributed to the mislocalization of N-cadherin and β-catenin, which then impacts on the Wnt signaling pathway. Higher levels of POPX2 are observed in more invasive breast cancer cell lines (Susila et al., 2010) and POPX2 has also been linked to the regulation of MAP kinases, ERK1/2 and glycogen synthase kinases, GSK3α, β (Zhang et al., 2013). The modulation of the KIF3 motor complex (this study) may add an additional complexity to POPX2's link to the regulation of cancer biology. POPX2 may regulate cancer cell behavior by inhibiting proper localization of N-cadherin and β-catenin to the cell periphery leading to their accumulation in other cellular compartments, which in turn affects other signaling pathways. The resultant loss of cell-cell contact can also be conducive to the dissemination of cancer cells during metastasis.

MATERIALS AND METHODS

Antibodies and plasmid constructs

Mouse monoclonal antibody to FLAG-M2, rabbit polyclonal antibody to FLAG and rabbit polyclonal antibody to β-catenin were purchase from Sigma-Aldrich. Mouse monoclonal antibodies against KAP3 were obtained from BD Biosciences and SantaCruz Biotechnology, respectively. Mouse monoclonal antibody to KIF3A and mouse monoclonal antibody to N-cadherin were from BD Biosciences. Rabbit polyclonal antibody to GFP was from Life Technologies. Rabbit polyclonal antibody to GST was from Bethyl laboratories Inc (Montgomery, TX, USA). Rabbit polyclonal antibody against phospho-serine/threonine was from ECM Biosciences (Versailles, KY, USA). Mouse monoclonal antibody to actin was from Chemicon (Millipore). Rabbit anti-sera against human POPX2 were from Koh's lab. Constructs encoding POPX2 and the phosphatase-dead mutant, POPX2m were described in Koh *et al* (Koh et al., 2002). Full length FLAG-tagged and GST-tagged KAP3 constructs were generated in the pXJ40 vector. Deletion mutants of KAP3 were constructed by cloning the PCR fragment generated with primers targeting various regions. Constructs encoding ORF of KIF3A were cloned into the pXJ40 vector containing their respective tags. KIF3A-S690A and KIF3A-S690D mutants were generated using

the QuikChange Site-directed mutagenesis kit (Stratagene-Agilent Technologies, Santa Clara, CA, USA). The motor domain of KIF3A (1-354) was amplified by PCR and cloned into the pXJ40 vector with FLAG tag. N-cadherin-eGFP (Addgene plasmid 18870) construct was from Addgene (Cambridge, MA, USA). The cDNA constructs of CaMKIIα were made in the pXJ40 vector with their respective tags. The original cDNA for KAP3 was a gift from Prof Yoshimi Takai. dsRed-Rab11a and mCherry-clathrin-LCA were kind gifts from Dr. Boon Chuan Low and Dr. Lei Lu, respectively. The cDNA of CaMKII was a gift from Dr Thomas Leung.

The accession numbers of the various genes/proteins used in this study are listed below: KIF3A (human), BC045542; KIF3B (mouse), NM_008444.4; KAP3 (human), NM_014970; POPX2 (human), AF520615; POPX1 (human): AF520614.

Cell culture, transfection and retrovirus infection

COS7 and NIH3T3 cells were grown in DMEM high glucose medium supplemented with 10% FBS. HeLa cells were maintained in minimal essential medium with 10% FBS. The cells were transiently transfected with Lipofectamine 2000 (Life Technologies) according to manufacturer's protocol. For stable transfections, GFP-tagged POPX2, POPX2m, KIF3A, KIF3A-S690A and KIF3A-S690D cDNAs were subcloned into the retroviral vector pBABE-puro, respectively. The packaging line, Phoenix-Eco cells, was transfected with various pBABE-puro plasmids using Lipofectamine 2000. The cells were cultured for more than 24 hrs and the supernatants were used to infect the NIH3T3 cells in the presence of 8 μg/ml of polybrene. Infected cells were selected and maintained in puromycin containing medium.

Immunofluorescence staining and time-lapse imaging

Cells on coverslips were fixed in 4% paraformaldehyde 24 hrs post transfection. The cells were then permeabilized in 0.2% Triton X-100 and blocked with 4% BSA. The cells were incubated with primary antibody in 1% Triton X-100 (1: 100) at 4 ℃ overnight, followed by incubation with secondary antibody in 1% Triton X-100 (1: 100) at room temperature for 1 hr. Coverslips were dried and mounted using Vectorshield with DAPI to show nuclei.

Carl Zeiss axiovert microscope and Zeiss objective Plan Neo-fluar 100X/1.3 oil or Plan-Apochromat 63X/1.4 were used. The MetaMorph software programme was used to capture images using a Roper Scientific CoolSNAP CCD camera. Time-lapse epi-fluorescence microscopy was performed on Carl Zeiss axiovert microscope equipped with Zeiss objective Plan Neo-fluar 100X/1.3 oil immersion objective, sample heater (37 °C) and CO_2 incubation chamber. Images were captured with Roper Scientific CoolSNAP CCD camera. Two different frame rates were used: 1 frame/3s (for all movies and figures except otherwise stated) or 2 frames/s (for Figures 4I, 7B, S4). An automated particle tracking software was used to analyse the images (see below). The play-back rate for all movies is 7 frames/s.

Cell aggregation assay

Cells were trypsinized in HBS (with or without 2 mM $CaCl_2$), followed by two washes in the respective HBS supplemented with 1% BSA and passed through a 27G needle thrice to obtain single cells. Cells were then diluted to 5 x 10^5 cell/ml in the same buffer and were incubated in 1.5 ml tubes at 37 ^{0}C with gentle rotation. After 30 mins, the number of cell particles was counted to determine the aggregation index (N_0–N_{30})/N_0, where N_{30} is the total particle number after 30 min incubation and N_0 is the total particle number at the start of incubation (Ozawa et al., 1990). Images of cell particles on the haemocytometer were captured with phase-contrast microscopy.

In vitro kinase & phosphatase assays

FLAG-CaMKII was expressed in COS7 cells and subjected to FLAG-immunoprecipitation. Activation of CaMKII was performed by adding kinase buffer (50 mM Tris pH 7.5, 10 mM $MgCl_2$, 5 mM $MnCl_2$, 1 mM dithiothreitol and 0.05% Triton X-100) supplemented with 1.2 µM calmodulin, 2 mM $CaCl_2$ and 200 µM ATP. The activation reaction was incubated at 30 ^{0}C for 10 mins. Kinase assays were performed by adding 8 µg of purified GST-fusion protein to the activated FLAG-CaMKII, in 30 µl of kinase buffer supplemented with 200 µM ATP. The kinase reaction (30 °C, 30 mins) was stopped by the addition of SDS sample buffer. For phosphatase assays, GST-KIF3A-Tail phosphorylated by CaMKII, was incubated with bacterially expressed POPX2 or CIP (New England Biolabs, Ipswich, MA, USA) for 30 mins at 30 °C. The reactions were stopped by the addition of SDS sample buffer.

Microtubule binding assay

Binding of KIF3A and its mutants to microtubules was assayed using the microtubule binding protein spin down assay kit (Cytoskelton Inc., Denver, CO, USA). KIF3A proteins were first immunoprecipitated and eluted using low pH glycine buffer, followed by neutralization with Tris buffer. Same amounts of eluted KIF3A proteins were incubated (as indicated by the input blot) with in vitro polymerized microtubules at room temperature for 30min. Microtubule bound and soluble proteins were separated by centrifugation. The microtubule fraction (pellet) was collected and analyzed by western blotting.

Automated particle tracking

The particle segmentation and tracking algorithms used in this paper are described in Lowe and Jaqaman et al., respectively (Lowe, 2004; Jaqaman et al., 2008). These algorithms are implemented through the Trackmate plugin in Fiji (Schindelin et al., 2012). Briefly, the particles within cells in each image of the time-lapsed sequence are segmented and identified using the difference of Gaussians approach (Lowe, 2004). These particles are then filtered based on quality and mean intensity. Next, the segmented particles are tracked by linking the individual particles from frame-to frame using the Linear Assignment Problem (LAP) method (Jaqaman et al., 2008), with modifications to the linking cost calculations with respect to both quality and mean intensity. The velocities of individual particles are then obtained from the particles tracks within the time-lapsed images. The particle tracks were then filtered based on their directional persistence in movement to eliminate particles that were not persistently moving in a particular direction. At any point in time, the mean squared displacement of a tracked particle with 2-dimensional coordinates *x* and y, is denoted as (r^2), where $r^2 = x^2 + y^2$. We describe the movement of each particle with $(r^2) \propto t^{\gamma}$, where *t* is the time elapsed since the start of particle tracking and γ is denoted as a particle movement persistence factor. When $\gamma = 1$, then $(r^2) \propto t$, where the displacement is proportional to the square root of the elapsed time and the particle is said to exhibit a random movement behaviour. When $\gamma = 2$, then $(r^2) \propto t^2$, where the displacement is proportional to the elapsed time and the particle exhibits directed

movement persistence. Hence, particle movement persistence can be quantified using γ, and particles with $\gamma \geq 1.3$ were retained.

ACKNOWLEDGEMENT

This study was supported by the Academic Research Fund Tier2 [grant number MOE2012-T2-1-046 to C.G.K.] and the Biomedical Research Council, Singapore [grant number 10/1/22/19/659 to C.G.K.]. We also thank the National Research Foundation, Singapore.

CONFLICT OF INTEREEST

The authors declare no conflict of interest.

AUTHOR CONTRIBUTIONS

H.Q.P., J.L.H. and S.K.L. performed the experiments and analyzed the data. Y.Z. and K.H.C. analyzed the data for particle tracking. H.Q.P., H.Y.L., and C.G.K. conceived and designed the experiments. C.G.K. wrote the manuscript.

FIGURE LEGEND

Fig. 1. Interaction of POPX with KAP3. (**A**) Association of endogenous KAP3 with GFP-POPX2. KAP3 was immunoprecipitated from control (NIH3T3) and stable GFP-POPX2-overexpressing-NIH3T3 (X2) cell lysates and subjected to Western analysis with the indicated antibodies. Mouse random IgG was used to demonstrate absence of non-specific binding. (**B**) Association of KAP3 with POPX1. Plasmid encoding FLAG-KAP3 was co-transfected with full length GST-POPX1 or its truncation mutants (illustrated on panel at the right). The lysates were subjected to GST pull-down assay and the precipitated proteins were resolved by SDS-PAGE followed by Western blot analysis with the indicated antibodies. (**C**) Mapping the KAP3 binding region in POPX2. Experiments were done as in (B). **(D)** KAP3 armadillo repeats are required for interaction with POPX2. FLAG-tagged constructs consisting of various regions of the KAP3 armadillo repeats were tested for their ability to bind GST-POPX2 in the GST pull-down assay.

Fig. 2. POPX2 overexpression affects localization of N-cadherin and β-catenin to the cell periphery. Representative images of immunostaining of parent NIH3T3 (Ctrl) and X2 cells with (**A**) anti-N-cadherin and Dapi, (**B**) anti-β-catenin and Dapi. Scale bar: 20 μm. (**C**) Total protein levels of N-cadherin and β-catenin in the Ctrl and X2 cells were analyzed by Western analysis with the indicated antibodies. **(D)** There are less surface N-cadherin proteins in X2 cells. Total surface proteins were biotinylated and then harvested by streptavidin resins. The surface proteins were then analyzed by SDS-PAGE using anti-N-cadherin antibodies. Actin was used as loading control. (**E**) Interaction between N-cadherin and KAP3 is not affected by POPX2. Cell lysates of the Ctrl and X2 cells were subjected to immunoprecipitation with anti-N-cadherin or anti-KAP3 antibodies. The immunoprecipitated complexes were eluted, resolved by SDS-PAGE and immunoblotted with the indicated antibodies. (**F**) Interaction between KIF3A and KAP3 is not affected by POPX2. The parent NIH3T3 cells (Ctrl) and X2 cells were transfected with FLAG-KIF3A or FLAG vector. The cell lysates were subjected to FLAG immunoprecipitation and the co-IP complexes were separated by SDS-PAGE and immunoblotted with the indicated antibodies.

Fig. 3. POPX2 phosphatase activity affects N-cadherin/β-catenin localization and cell-cell adhesion. Representative images of immunostaining of NIH3T3 cells infected with retroviral vector encoding GFP, GFP-POPX2 or GFP-POPX2m. Cells were double-stained with (**A**) anti-N-cadherin antibodies and Dapi, or (**B**) anti-β-catenin antibodies and Dapi. Scale bar: 20 μm. (**C, D**) Cell-cell adhesion is inhibited in POPX2-overexpressing cells. The retrovirus infected cell lines were subjected to aggregation assay in the following conditions: 2 mM $CaCl_2$, 2mM $CaCl_2$ + 2 mM EGTA, no $CaCl_2$. (**C**) Representative images of the assays taken under phase-contrast microscope are shown. Scale bar: 100 μm. (**D**) The level of cell aggregation was calculated by the aggregation index. Briefly, aggregation index = $(N_0/N_{30})/N_0$, where N_0 is the total particle number at the start of incubation and N_{30} is the total particle number after 30 min incubation. Data shown are averages of three independent assays. Error bars represent standard deviations. $P < 0.001$.

Fig. 4. KIF3-motor mediated transport is impaired in POPX2-overexpressing cells. (**A**) N-cadherin-GFP was co-transfected with mCherry, mCherry-POPX2 or mCherry-POPX2m plasmids into NIH3T3 cells. Motility of N-cadherin-GFP in live cells was tracked using an automated particle tracking algorithm (see Materials and Methods). All N-cadherin-GFP particles in randomly selected cells were tracked. Ten colored coded representative tracks are shown for each case here. The experiment was repeated three times. Scale bar: 20 μm. (**B**) Measurement of mean velocity of N-cadherin-GFP from (A) (Mean ± S.D.; $^{**}P < 0.01$, Student's t-test). Number of particles ≥ 1713 for each case. Number of cells ≥ 5. Error bars denote standard deviation. $\gamma = 1.3$ for the results shown here. (**C**) dsRed-Rab11a was co-transfected with GFP, GFP-POPX2 or GFP-POPX2m plasmids into HeLa cells. Motility of dsRed-Rab11a vesicles in live cells was tracked using an automated particle tracking algorithm. All dsRed-Rab11a vesicles in each cell were tracked. Ten colored coded representative tracks are shown for each case here. .The experiment was repeated three times. Scale bar: 20 μm. (**D**) Measurement of mean velocity of dsRed-Rab11a vesicles from (C) (Mean ± S.D.; $^{**}P < 0.01$; Student's t-test). Number of particles ≥ 1145 for each case. Number of cells ≥ 4. Error bars denote standard deviation. $\gamma = 1.3$ for the results shown here. (**E**) dsRed-Rab11a was co-transfected with GFP, GFP-

POPX2 or GFP-POPX2m plasmids into HeLa cells. After 24 hours, cells were fixed and imaged by fluorescent microscopy. (**F**) Scoring of cells showing the three phenotypes (normal, clustered, highly clustered) depicted in (E). Data are averages of three independent experiments, n = 50. Scale bar: 20 μm. (**G**) Clathrin-LCA-mCherry was co-transfected with GFP, GFP-POPX2 or GFP-POPX2m plasmids into HeLa cells. Motility of clathrin-LCA-mCherry vesicles in live cells was tracked using an automated particle tracking algorithm. Ten colored coded representative tracks are shown for each case here. Five cells were randomly selected and all vesicles in each cell were tracked. The experiment was repeated three times. Scale bar: 20 μm. (**H**) Measurement of mean velocity of clathrin-LCA-mCherry vesicles from (G). Number of particles ≥ 1292. **(I)** Trafficking of mitochondria was not affected by POPX2. Mitochondria were labeled with MitoTracker Red CMXRos in control and GFP-POPX2 expressing cells. Movement of mitochondria was determined by tracking the edges of mitochondria using Zeiss imaging software. 50 mitochondria edges were tracked in each experiment. 3 independent experiments were performed. Error bar: standard deviation.

Fig. 5. Mutation of KIF3A-serine-690 results in impaired KIF3 cargo transport. (**A**) Domain organization of KIF3A is shown in the upper panel. Serine 690 (S690) is located in the C-terminal tail of KIF3A. The alignment of 15 amino acid residues in the C-terminal tails of human, mouse and zebrafish is shown in the lower panel. The conserved putative consensus sequence for CaMKII is highlighted in yellow. (**B**) Representative images of immunostaining of NIH3T3 cells infected with retroviral vector encoding GFP, GFP-KIF3A-S690A or GFP-KIF3A-S690D. Cells were double-stained with anti-N-cadherin antibodies and Dapi. Scale bar: 20 μm. **(C)** There is less surface N-cadherin in KIF3A-S690A overexpressing cells. Total surface N-cadherin was assayed as in Fig. 2D. (**D**) N-cadherin-GFP was co-transfected with mCherry-KIF3A, mCherry-KIF3A-S690A or mCherry-KIF3A-S690D plasmids into NIH3T3 cells. Motility of N-cadherin-GFP vesicles in live cells was tracked using. an automated particle tracking algorithm. Ten colored coded representative tracks are shown for each case here. Five cells were randomly selected all vesicles from each cell were tracked. The experiment was repeated three times. Scale bar: 20 μm. (**E**) Measurement of mean velocity of N-cadherin-GFP vesicles from (D). Number of

particles ≥ 1196. γ = 1.3 for the results shown here. (Mean ± S.D.; **P < 0.01, Student's t-test). (**F**) dsRed-Rab11a was co-transfected with GFP-KIF3A, GFP-KIF3A-S690A or GFP-KIF3A-S690D into HeLa cells. Motility of dsRed-Rab11a vesicles in live cells was tracked using an automated particle tracking algorithm. Ten colored coded representative tracks are shown for each case here. Five cells were randomly selected and all vesicles from each cell were tracked. The experiment was repeated three times. Scale bar: 20 μm. (**G**) Measurement of mean velocity of dsRed-Rab11a vesicles from (F). Number of particles ≥ 1145. γ = 1.3 for the results shown here. (Mean ± S.D.; ***P* < 0.01, Student's t-test).

Fig. 6. Phosphorylation of KIF3A-S690 is regulated by CaMKII. (**A**) Mutation of KIF3A serine-690 does not affect binding of KIF3A to KAP3. GST-KAP3 was co-transfected with FLAG-KIF3A, FLAG-KIF3A-S690A or FLAG-KIF3A-S690D plasmids. KIF3A was immunoprecipitated with anti-FLAG antibodies. The bound proteins were resolved by SDS-PAGE and immunoblotted with the indicated antibodies. (**B**) Interaction between the motor and tail domain of KIF3A. Plasmid encoding FLAG-KIF3A-Motor was co-transfected with GST-KIF3A-Tail, GST-S690A-Tail, GST-690D-Tail or GST plasmids into COS-7 cells. The lysates were subjected to GST pull-down and precipitated proteins were separated by SDS-PAGE gel followed by Western analysis using the indicated antibodies. **(C)** Microtubule binding assay. Similar amounts of FLAG-KIF3A-WT, FLAG-KIF3A-S690A and FLAG-KIF3A-S690D proteins (lower panel) were incubated with microtubules. After centrifugation, the pellet which contained the microtubules was analyzed by SDS-PAGE and Western using the indicated antibodies. Less KIF3A-S690A was found to be associated with the microtubules (top panel). Similar amounts of microtubules were found in the pellets (middle panel, coomassie blue stained bands). (**D**) *In vitro* kinase assay. The tail domains of wild type KIF3A and S690A mutant were expressed as recombinant GST fusion proteins in the *E.coli* cells. FLAG-CaMKII and active FLAG-PAK1 were harvested from transfected COS7 cells. FLAG-CaMKII was activated *in vitro* by calcium and calmodulin. GST fusion proteins were added to active FLAG-PAK1, inactive FLAG-CaMKII and active FLAG-CaMKII, respectively and were subjected to *in vitro* kinase assay. The proteins were resolved on SDS-PAGE and analyzed by Western with the indicated antibodies. Lane 1: active FLAG-

PAK1 + GST-KIF3A-Tail; 2: inactive FLAG-CaMKII + GST-KIF3A-Tail; 3: active CaMKII + GST-KIF3A-Tail; 4: active FLAG-CaMKII + GST-S690A-Tail.

Fig. 7. KIF3-motor mediated transport is impaired in the presence of CaMKII inhibitors. (**A**) N-cadherin-GFP was transfected into NIH3T3 cells. CaMKII inhibitor KN-93 (10 μM) was included to monitor the effects on N-cadherin trafficking. The motility of N-cadherin-GFP was tracked using an automatic tracking algorithm. Ten colored coded representative tracks are shown for each case here. Cells were randomly selected and all vesicles in each cell were tracked. The experiment was repeated three times. Scale bar: 20 μm. **(B)** Additional CaMKII inhibitors, AIP (10 μM) and KN-62 (15 μM), were included to monitor the effects on N-cadherin trafficking. N-cadherin-GFP plasmid was transfected into HeLa cells. The motility of N-cadherin-GFP was tracked using an automatic tracking algorithm. Ten colored coded representative tracks are shown for each case here. (**C**) Measurement of mean velocity of N-cadherin-GFP vesicles from (A) (Mean ± S.D.; *P< 0.01; Student's t-test). Number of particles ≥ 1247 for each case. Error bars denote standard deviation. $\gamma = 1.3$ for the results shown here. **(D)** Additional CaMKII inhibitors, AIP (10 μM) and KN-62 (15 μM), resulted in impaired N-cadherin trafficking. Mean velocity of N-cadherin-GFP was calculated from (B) (Mean ± S.E.; **P< 0.01; Student's t-test). Number of particles ≥ 939 for each case, Error bars denote standard deviation. $\gamma = 1.3$ for the results shown here. (**E**) *In vitro* phosphatase assay. CaMKII phosphorylated GST-KIF3A-Tail was incubated with bacterial expressed GST-POPX2 or calf intestinal phosphatase, CIP. The reaction mixtures were then resolved by SDS-PAGE and subjected to Western analysis using the indicated antibodies. Lane 1: non-phosphorylated GST-KIF3A-Tail alone (negative control); 2: phosphorylated GST-KIF3A-Tail alone (positive control); 3: phosphorylated GST-KIF3A-Tail + GST-POPX2; 4: phosphorylated GST-KIF3A-Tail + CIP. (**F**) Pre-phosphorylated GST-KIF3A-tail fusion protein was incubated with various phosphatases harvested from transfected COS7 cells (See Fig. S2C for protein purity). The reaction mix was separated by SDS-PAGE followed by Western analysis using anti-phospho-Ser/Thr antibodies. Lane 1: non-phosphorylated GST-KIF3A-Tail; 2: phosphorylated GST-KIF3A-Tail; 3: phosphorylated GST-KIF3A-Tail + GST-POPX2; 4: phosphorylated

GST-KIF3A-Tail + GST-PP2C; 5: phosphorylated GST-KIF3A-Tail + GST-PP1.

Fig. 8. Silencing POPX2 does not affect N-cadherin trafficking. **(A)** NIH3T3 cells were transfected with siRNA targeting luciferase (as control) and POPX2. The transfected cells were fixed and stained with anti-N-cadherin and DAPI. Scale bar: 20 μm **(B)** NIH3T3 cells were co-transfected with N-cadherin-GFP cDNA and siRNA targeting luciferase (control) or POPX2. N-cadherin-GFP were tracked using an automatic tracking algorithm. Ten colored coded representative tracks are shown for each case here.. Five cells were randomly selected and all vesicles from each cell were tracked. The experiment was repeated three times. Scale bar: 20 μm. **(C)** Measurement of mean velocity of N-cadherin-GFP vesicles from (B). Number of particles $\geq$ 732. Error bars represent standard deviation. $\gamma = 1.3$ for the results shown here. **(D)** RT-PCR shows about 50% knockdown of POPX2 transcript in X2 cells.

REFERENCES

Ballif, B. A., Villen, J., Beausoleil, S. A., Schwartz, D. and Gygi, S. P. (2004). Phosphoproteomic analysis of the developing mouse brain. *Mol. Cell. Proteomics* **3**, 1093-1101.

Cahu, J., Olichon, A., Hentrich, C., Schek, H., Drinjakovic, J., Zhang, C., Doherty-Kirby, A., Lajoie, G. and Surrey, T. (2008). Phosphorylation by Cdk1 increases the binding of Eg5 to microtubules in vitro and in Xenopus egg extract spindles. *PloS one* **3**, e3936.

Dephoure, N., Zhou, C., Villen, J., Beausoleil, S. A., Bakalarski, C. E., Elledge, S. J. and Gygi, S. P. (2008). A quantitative atlas of mitotic phosphorylation. *P. Natl. Acad. Sci. USA* **105**, 10762-10767.

Endow, S. A., Kull, F. J. and Liu, H. (2010). Kinesins at a glance. *J. Cell Sci.* **123**, 3420-3424.

Espeut, J., Gaussen, A., Bieling, P., Morin, V., Prieto, S., Fesquet, D., Surrey, T. and Abrieu, A. (2008). Phosphorylation relieves autoinhibition of the kinetochore motor Cenp-E. *Mol. Cell* **29**, 637-643.

Friedman, D. S. and Vale, R. D. (1999). Single-molecule analysis of kinesin motility reveals regulation by the cargo-binding tail domain. *Nat. Cell Biol.* **1**, 293-297.

Guillaud, L., Wong, R. and Hirokawa, N. (2008). Disruption of KIF17-Mint1 interaction by CaMKII-dependent phosphorylation: a molecular model of kinesin-cargo release. *Nat. Cell Biol.* **10**, 19-29.

Hammond, J. W., Blasius, T. L., Soppina, V., Cai, D. and Verhey, K. J. (2010). Autoinhibition of the kinesin-2 motor KIF17 via dual intramolecular mechanisms. *J.l Cell Biol.* **189**, 1013-1025.

Hirokawa, N. (2000). Stirring up development with the heterotrimeric kinesin KIF3. *Traffic* **1**, 29-34.

Hirokawa, N., Nitta, R. and Okada, Y. (2009). The mechanisms of kinesin motor motility: lessons from the monomeric motor KIF1A. *Nat. Rev. Mol. Cell Biol.* **10**, 877-884.

Huttlin, E. L., Jedrychowski, M. P., Elias, J. E., Goswami, T., Rad, R., Beausoleil, S. A., Villen, J., Haas, W., Sowa, M. E. and Gygi, S. P. (2010). A tissue-specific atlas of mouse protein phosphorylation and expression. *Cell* **143**, 1174-1189.

Ichimura, T., Wakamiya-Tsuruta, A., Itagaki, C., Taoka, M., Hayano, T., Natsume, T. and Isobe, T. (2002). Phosphorylation-dependent interaction of kinesin light chain 2 and the 14-3-3 protein. *Biochemistry* **41**, 5566-5572.

Ishida, A., Kameshita, I. and Fujisawa, H. (1998). A novel protein phosphatase that dephosphorylates and regulates Ca2+/calmodulin-dependent protein kinase II. *J. Biol. Chem.* **273**, 1904-1910.

Jang, Y. N., Jung, Y. S., Lee, S. H., Moon, C. H., Kim, C. H. and Baik, E. J. (2009). Calpain-mediated N-cadherin proteolytic processing in brain injury. *J. Neurosci.* **29**, 5974-5984.

Jaqaman, K., Loerke, D., Mettlen, M., Kuwata, H., Grinstein, S., Schmid, S. L. and Danuser, G. (2008). Robust single-particle tracking in live-cell time-lapse sequences. *Nat. Methods* **5**, 695-702.

Jimbo, T., Kawasaki, Y., Koyama, R., Sato, R., Takada, S., Haraguchi, K. and Akiyama, T. (2002). Identification of a link between the tumour suppressor APC and the kinesin superfamily. *Nat. Cell Biol.* **4**, 323-327.

Kanemaru, K., Kubota, J., Sekiya, H., Hirose, K., Okubo, Y. and Iino, M. (2013). Calcium-dependent N-cadherin up-regulation mediates reactive astrogliosis and neuroprotection after brain injury. *P. Natl. Acad. Sci. USA* **110**, 11612-11617.

Koh, C. G., Tan, E. J., Manser, E. and Lim, L. (2002). The p21-activated kinase PAK is negatively regulated by POPX1 and POPX2, a pair of serine/threonine phosphatases of the PP2C family. *Curr. Biol.* **12**, 317-321.

Loubery, S., Wilhelm, C., Hurbain, I., Neveu, S., Louvard, D. and Coudrier, E. (2008). Different microtubule motors move early and late endocytic compartments. *Traffic* **9**, 492-509.

Lowe, D. G. (2004). Distinctive image features from scale-invariant keypoints. *Int. J. Comput. Vision* **60**, 91-110.

Manser, E., Loo, T. H., Koh, C. G., Zhao, Z. S., Chen, X. Q., Tan, L., Tan, I., Leung, T. and Lim, L. (1998). PAK kinases are directly coupled to the PIX family of nucleotide exchange factors. *Mol. Cell* **1**, 183-192.

Mary, S., Charrasse, S., Meriane, M., Comunale, F., Travo, P., Blangy, A. and Gauthier-Rouviere, C. (2002). Biogenesis of N-cadherin-dependent cell-cell contacts in living fibroblasts is a microtubule-dependent kinesin-driven mechanism. *Mol. Biol. Cell* **13**, 285-301.

Morfini, G. A., You, Y. M., Pollema, S. L., Kaminska, A., Liu, K., Yoshioka, K., Bjorkblom, B., Coffey, E. T., Bagnato, C., Han, D. et al. (2009). Pathogenic huntingtin inhibits fast axonal transport by activating JNK3 and phosphorylating kinesin. *Nat. Neurosci.* **12**, 864-871.

Olsen, J. V., Vermeulen, M., Santamaria, A., Kumar, C., Miller, M. L., Jensen, L. J., Gnad, F., Cox, J., Jensen, T. S., Nigg, E. A. et al. (2010). Quantitative phosphoproteomics reveals widespread full phosphorylation site occupancy during mitosis. *Sci. Signal.* **3**, ra3.

Ozawa, M., Ringwald, M. and Kemler, R. (1990). Uvomorulin-catenin complex formation is regulated by a specific domain in the cytoplasmic region of the cell adhesion molecule. *P. Natl. Acad. Sci. USA* **87**, 4246-4250.

Pan, C., Gnad, F., Olsen, J. V. and Mann, M. (2008). Quantitative phosphoproteome analysis of a mouse liver cell line reveals specificity of phosphatase inhibitors. *Proteomics* **8**, 4534-4546.

Schindelin, J., Arganda-Carreras, I., Frise, E., Kaynig, V., Longair, M., Pietzsch, T., Preibisch, S., Rueden, C., Saalfeld, S., Schmid, B. et al. (2012). Fiji: an open-source platform for biological-image analysis. *Nat. Methods* **9**, 676-682.

Schonteich, E., Wilson, G. M., Burden, J., Hopkins, C. R., Anderson, K., Goldenring, J. R. and Prekeris, R. (2008). The Rip11/Rab11-FIP5 and kinesin II complex regulates endocytic protein recycling. *J. Cell Sci.* **121**, 3824-3833.

Singh, P., Gan, C. S., Guo, T., Phang, H. Q., Sze, S. K. and Koh, C. G. (2011). Investigation of POPX2 phosphatase functions by comparative phosphoproteomic analysis. *Proteomics* **11**, 2891-2900.

Stock, M. F., Guerrero, J., Cobb, B., Eggers, C. T., Huang, T. G., Li, X. and Hackney, D. D. (1999). Formation of the compact confomer of kinesin requires a COOH-terminal heavy chain domain and inhibits microtubule-stimulated ATPase activity. *J. Biol. Chem.* **274**, 14617-14623.

Susila, A., Chan, H., Loh, A. X., Phang, H. Q., Wong, E. T., Tergaonkar, V. and Koh, C. G. (2010). The POPX2 phosphatase regulates cancer cell motility and invasiveness. *Cell cycle* **9**, 179-187.

Takeda, S., Yamazaki, H., Seog, D. H., Kanai, Y., Terada, S. and Hirokawa, N. (2000). Kinesin superfamily protein 3 (KIF3) motor transports fodrin-associating vesicles important for neurite building. *J. Cell Biol.* **148**, 1255-1265.

Tanuma, N., Nomura, M., Ikeda, M., Kasugai, I., Tsubaki, Y., Takagaki, K., Kawamura, T., Yamashita, Y., Sato, I., Sato, M. et al. (2009). Protein phosphatase Dusp26 associates with KIF3 motor and promotes N-cadherin-mediated cell-cell adhesion. *Oncogene* **28**, 752-761.

Teng, J., Rai, T., Tanaka, Y., Takei, Y., Nakata, T., Hirasawa, M., Kulkarni, A. B. and Hirokawa, N. (2005). The KIF3 motor transports N-cadherin and organizes the developing neuroepithelium. *Nat.Cell Biol.* **7**, 474-482.

Tweedie-Cullen, R. Y., Reck, J. M. and Mansuy, I. M. (2009). Comprehensive mapping of post-translational modifications on synaptic, nuclear, and histone proteins in the adult mouse brain. *J. Proteome Res.* **8**, 4966-4982.

Vagnoni, A., Rodriguez, L., Manser, C., De Vos, K. J. and Miller, C. C. (2011). Phosphorylation of kinesin light chain 1 at serine 460 modulates binding and trafficking of calsyntenin-1. *J. Cell Sci.* **124**, 1032-1042.

Wedaman, K. P., Meyer, D. W., Rashid, D. J., Cole, D. G. and Scholey, J. M. (1996). Sequence and submolecular localization of the 115-kD accessory subunit of the heterotrimeric kinesin-II (KRP85/95) complex. *J. Cell Biol.* **132**, 371-380.

Wisniewski, J. R., Nagaraj, N., Zougman, A., Gnad, F. and Mann, M. (2010). Brain phosphoproteome obtained by a FASP-based method reveals plasma membrane protein topology. *J. Proteome Res.* **9**, 3280-3289.

Wozniak, M. J. and Allan, V. J. (2006). Cargo selection by specific kinesin light chain 1 isoforms. *EMBO J.* **25**, 5457-5468.

Xie, Y., Tan, E. J., Wee, S., Manser, E., Lim, L. and Koh, C. G. (2008). Functional interactions between phosphatase POPX2 and mDia modulate RhoA pathways. *J. Cell Sci.* **121**, 514-521.

Zhang, S., Guo, T., Chan, H., Sze, S. K. and Koh, C. G. (2013). Integrative Transcriptome and Proteome Study to Identify the Signaling Network Regulated by POPX2 Phosphatase. *J. Proteome Res.* **12**, 2525-2536.

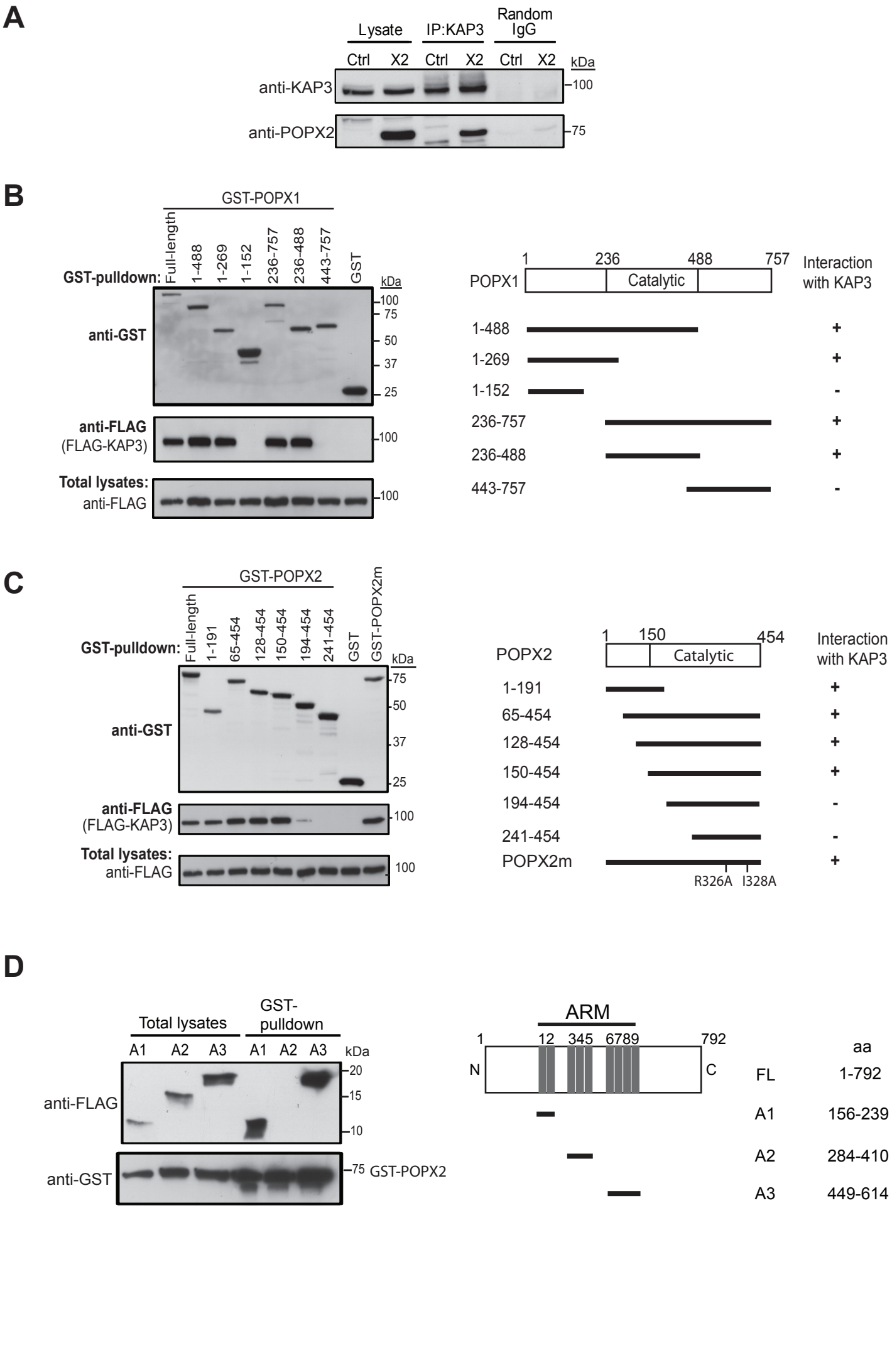
A
Lysate
IP:KAP3
Random IgG
Ctrl
X2
Ctrl
X2
Ctrl
X2
kDa
anti-KAP3
100
anti-POPX2
75
B
GST-POPX1
Full-length
1-488
1-269
1-152
236-757
236-488
443-757
GST
GST-pulldown:
kDa
100
75
50
37
25
anti-GST
anti-FLAG
(FLAG-KAP3)
100
Total lysates:
anti-FLAG
100
1
236
488
757
POPX1
Catalytic
Interaction with KAP3
1-488
+
1-269
+
1-152
-
236-757
+
236-488
+
443-757
-
C
GST-POPX2
GST-POPX2m
Full-length
1-191
65-454
128-454
150-454
194-454
241-454
GST
GST-pulldown:
kDa
75
50
37
25
anti-GST
anti-FLAG
(FLAG-KAP3)
100
Total lysates:
anti-FLAG
100
1
150
454
POPX2
Catalytic
Interaction with KAP3
1-191
+
65-454
+
128-454
+
150-454
+
194-454
-
241-454
-
POPX2m
+
R326A
I328A
D
Total lysates
GST-pulldown
A1
A2
A3
A1
A2
A3
kDa
20
15
10
anti-FLAG
anti-GST
75
GST-POPX2
ARM
1
12
345
6789
792
N
C
aa
FL
1-792
A1
156-239
A2
284-410
A3
449-614

Figure 1

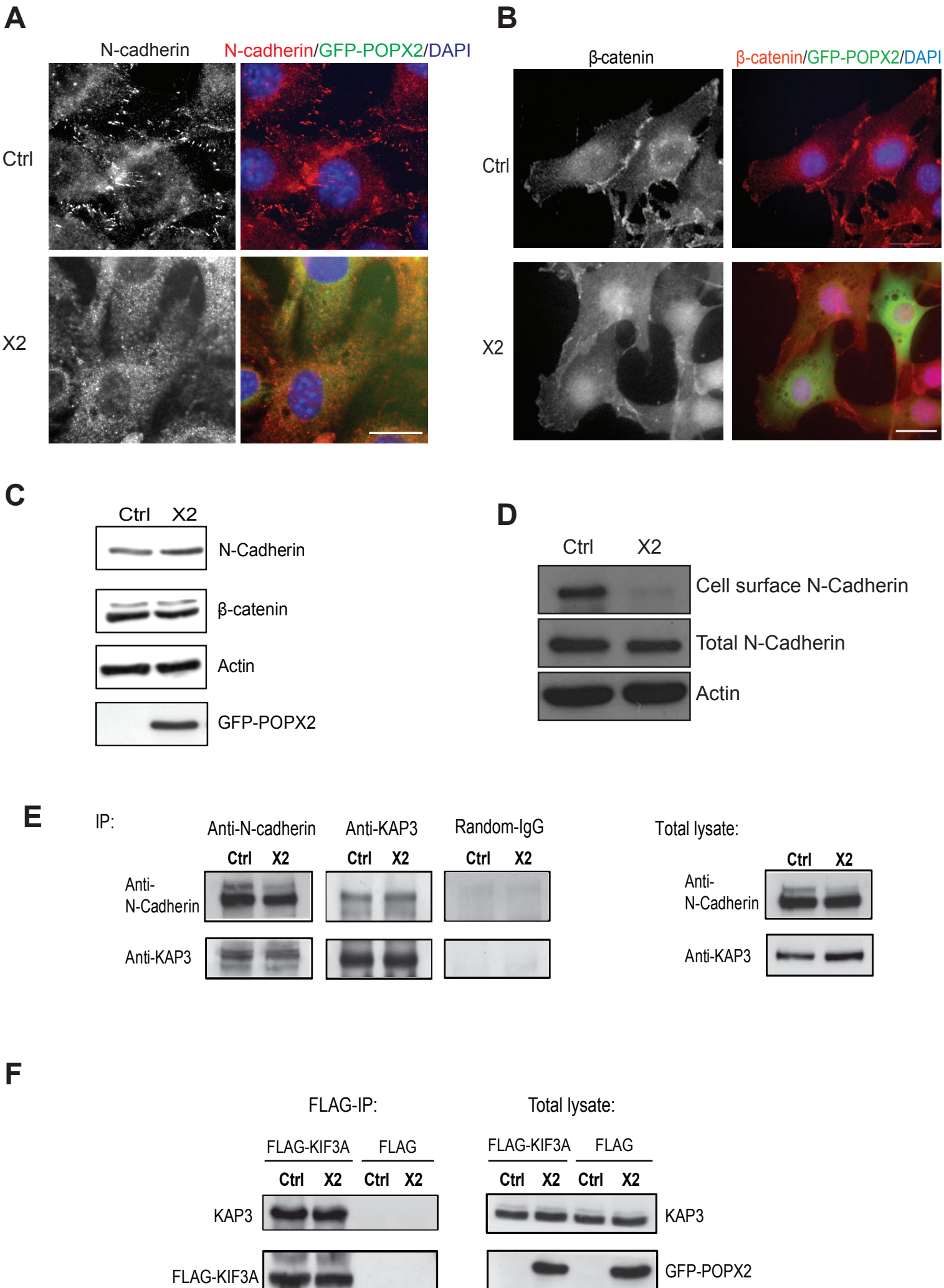
A
N-cadherin
N-cadherin/GFP-POPX2/DAPI
Ctrl
X2
B
β-catenin
β-catenin/GFP-POPX2/DAPI
Ctrl
X2
C
Ctrl X2
N-Cadherin
β-catenin
Actin
GFP-POPX2
D
Ctrl X2
Cell surface N-Cadherin
Total N-Cadherin
Actin
E
IP:
Anti-N-cadherin
Anti-KAP3
Random-IgG
Ctrl X2
Ctrl X2
Ctrl X2
Anti-
N-Cadherin
Anti-KAP3
Total lysate:
Ctrl X2
Anti-
N-Cadherin
Anti-KAP3
F
FLAG-IP:
Total lysate:
FLAG-KIF3A
FLAG
FLAG-KIF3A
FLAG
Ctrl X2 Ctrl X2
Ctrl X2 Ctrl X2
KAP3
FLAG-KIF3A
KAP3
GFP-POPX2

Figure 2

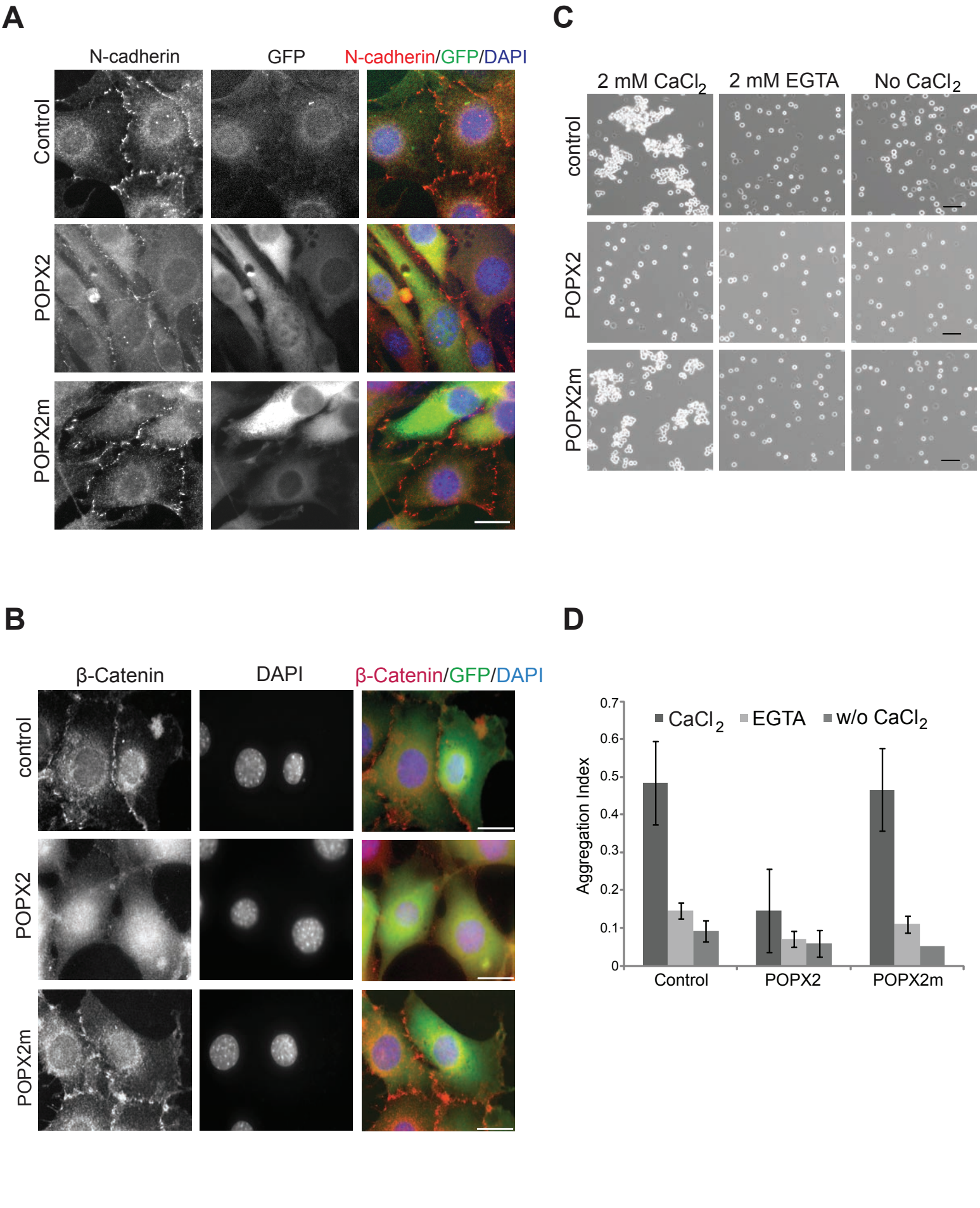
A
N-cadherin
GFP
N-cadherin/GFP/DAPI
Control
POPX2
POPX2m
B
β-Catenin
DAPI
β-Catenin/GFP/DAPI
control
POPX2
POPX2m
C
2 mM CaCl2
2 mM EGTA
No CaCl2
control
POPX2
POPX2m
D
CaCl2
EGTA
w/o CaCl2
Aggregation Index
0.7
0.6
0.5
0.4
0.3
0.2
0.1
0
Control
POPX2
POPX2m

Figure 3

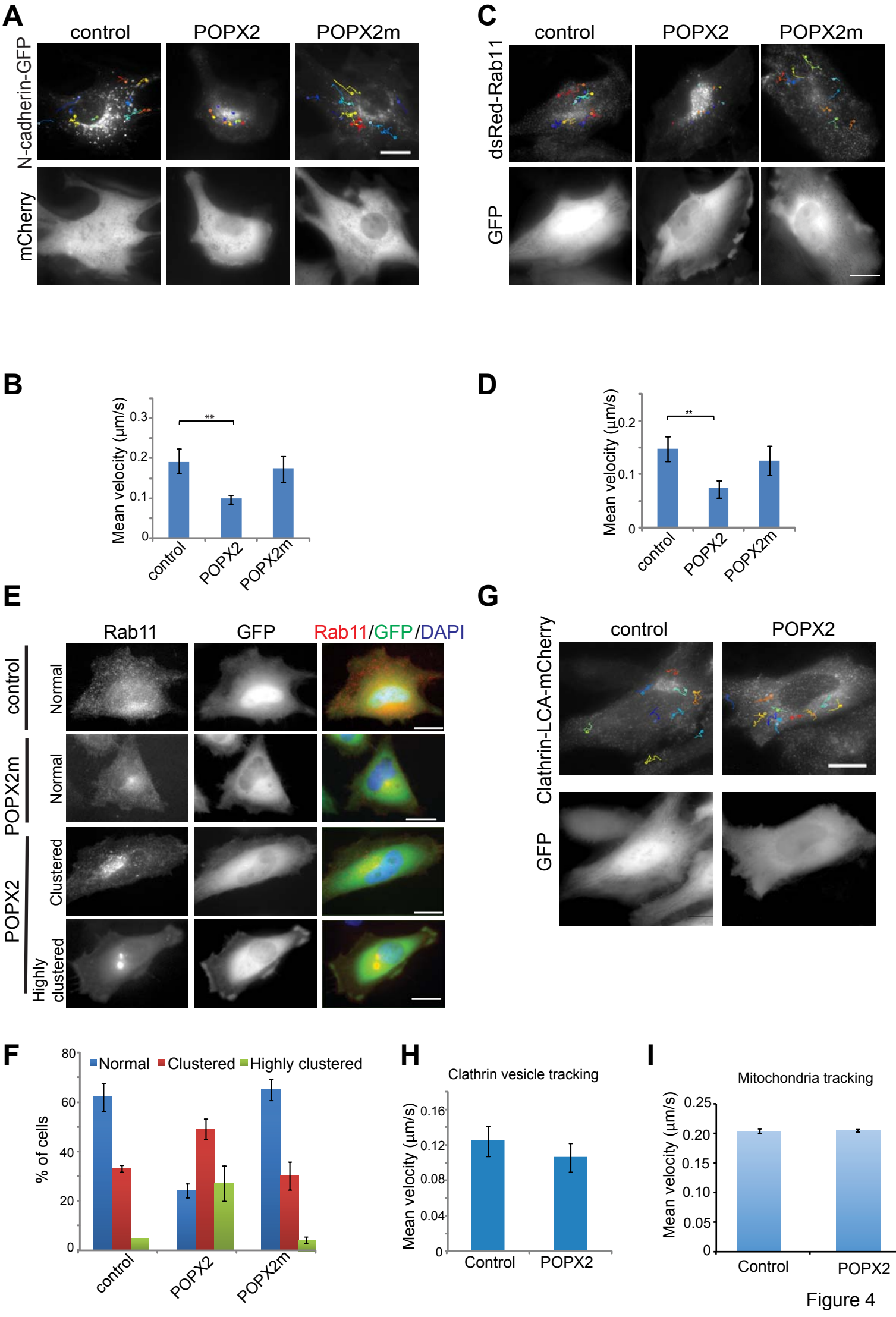
A
control
POPX2
POPX2m
N-cadherin-GFP
mCherry
C
control
POPX2
POPX2m
dsRed-Rab11
GFP
B
Mean velocity (μm/s)
0.3
0.2
0.1
0
**
control
POPX2
POPX2m
D
Mean velocity (μm/s)
0.2
0.1
0
**
control
POPX2
POPX2m
E
Rab11
GFP
Rab11/GFP/DAPI
control
Normal
POPX2m
Normal
POPX2
Clustered
Highly clustered
G
control
POPX2
Clathrin-LCA-mCherry
GFP
F
Normal
Clustered
Highly clustered
% of cells
80
60
40
20
0
control
POPX2
POPX2m
H
Clathrin vesicle tracking
Mean velocity (μm/s)
0.16
0.12
0.08
0.04
0
Control
POPX2
I
Mitochondria tracking
Mean velocity (μm/s)
0.25
0.20
0.15
0.10
0.05
0
Control
POPX2

Figure 4

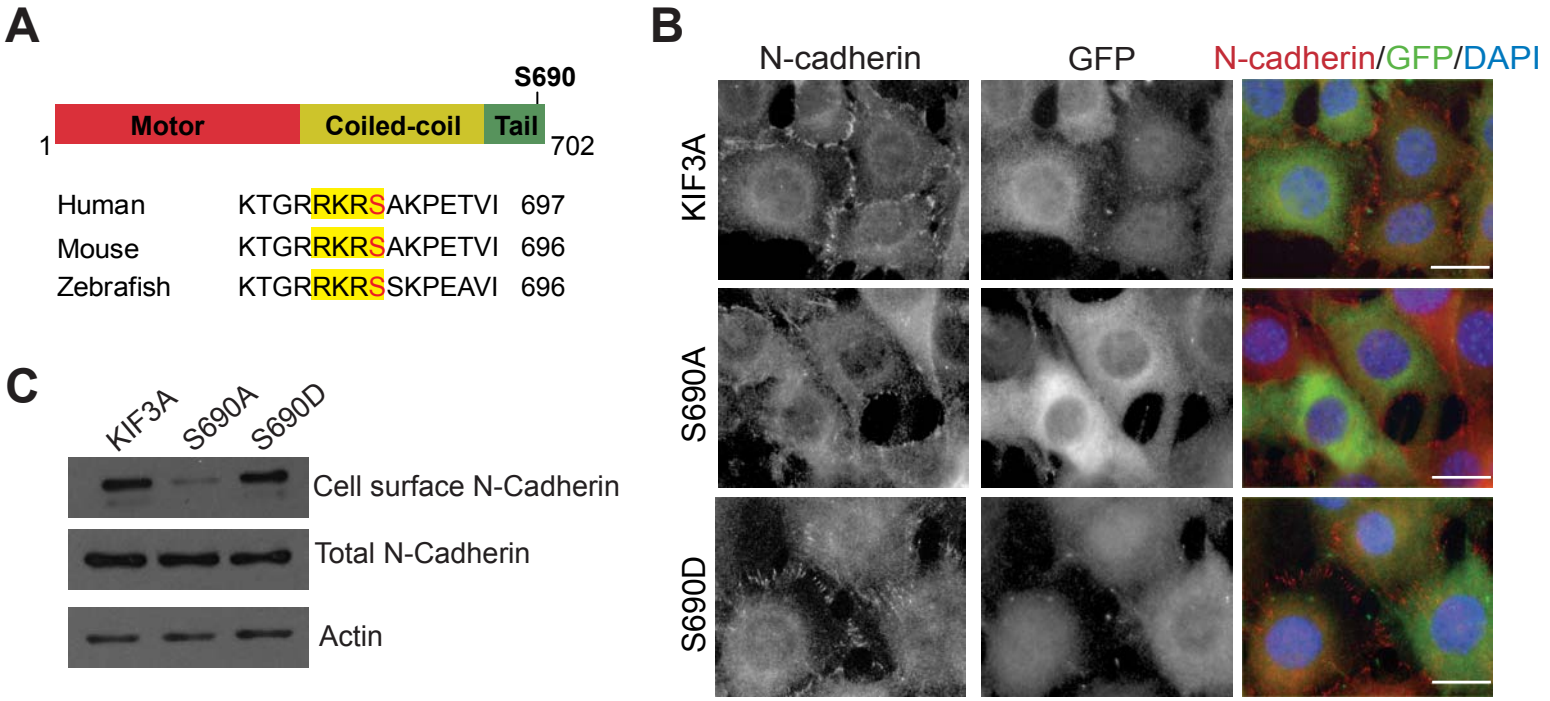
A
S690
Motor
Coiled-coil
Tail
1
702
Human KTGRRKRSAKPETVI 697
Mouse KTGRRKRSAKPETVI 696
Zebrafish KTGRRKRSSKPEAVI 696
B
N-cadherin
GFP
N-cadherin/GFP/DAPI
KIF3A
S690A
S690D
C
KIF3A
S690A
S690D
Cell surface N-Cadherin
Total N-Cadherin
Actin

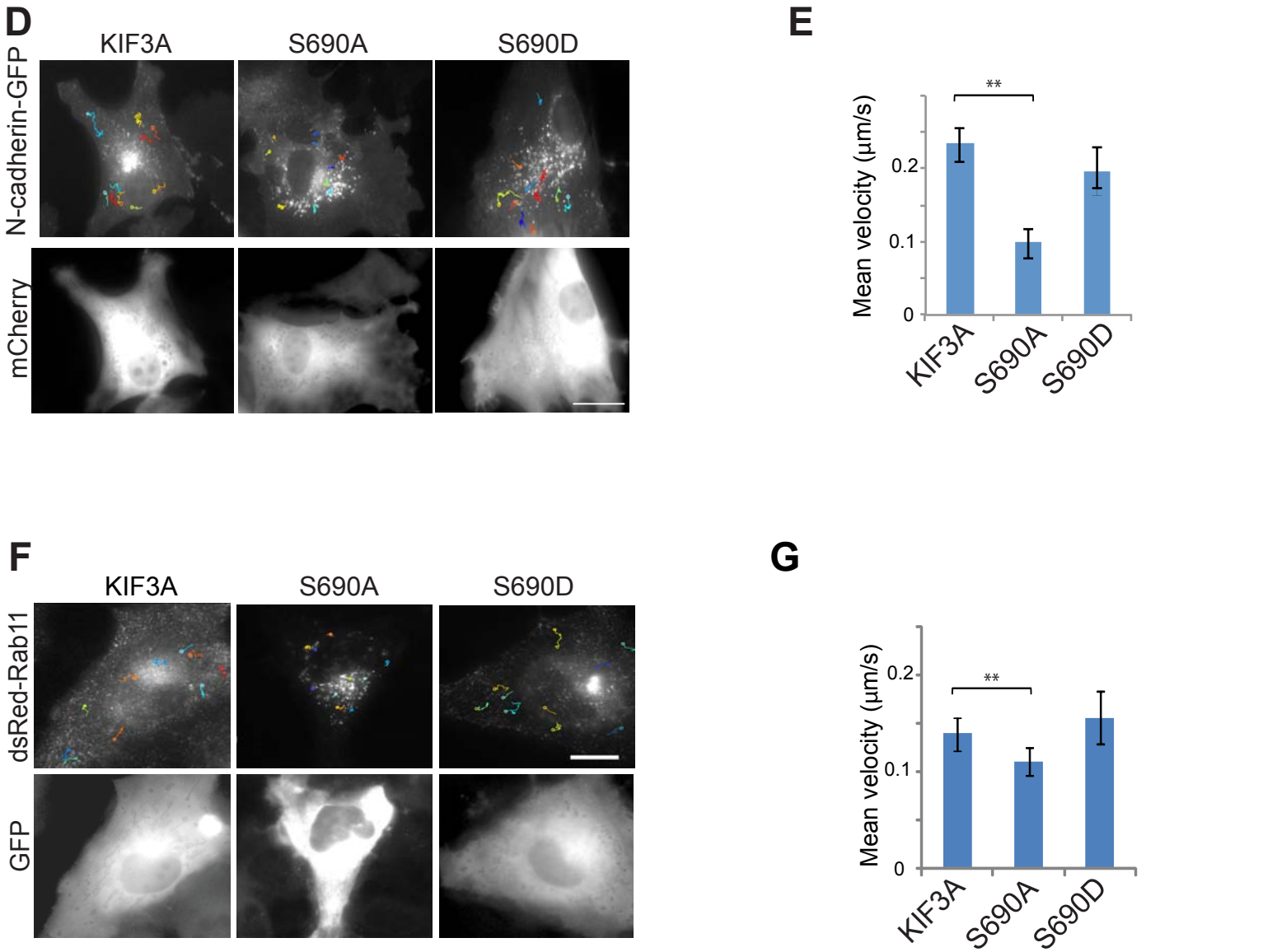
D
KIF3A
S690A
S690D
N-cadherin-GFP
mCherry
E
Mean velocity (μm/s)
**
0.2
0.1
0
KIF3A
S690A
S690D

F
KIF3A
S690A
S690D
dsRed-Rab11
GFP
G
Mean velocity (μm/s)
**
0.2
0.1
0
KIF3A
S690A
S690D

Figure 5

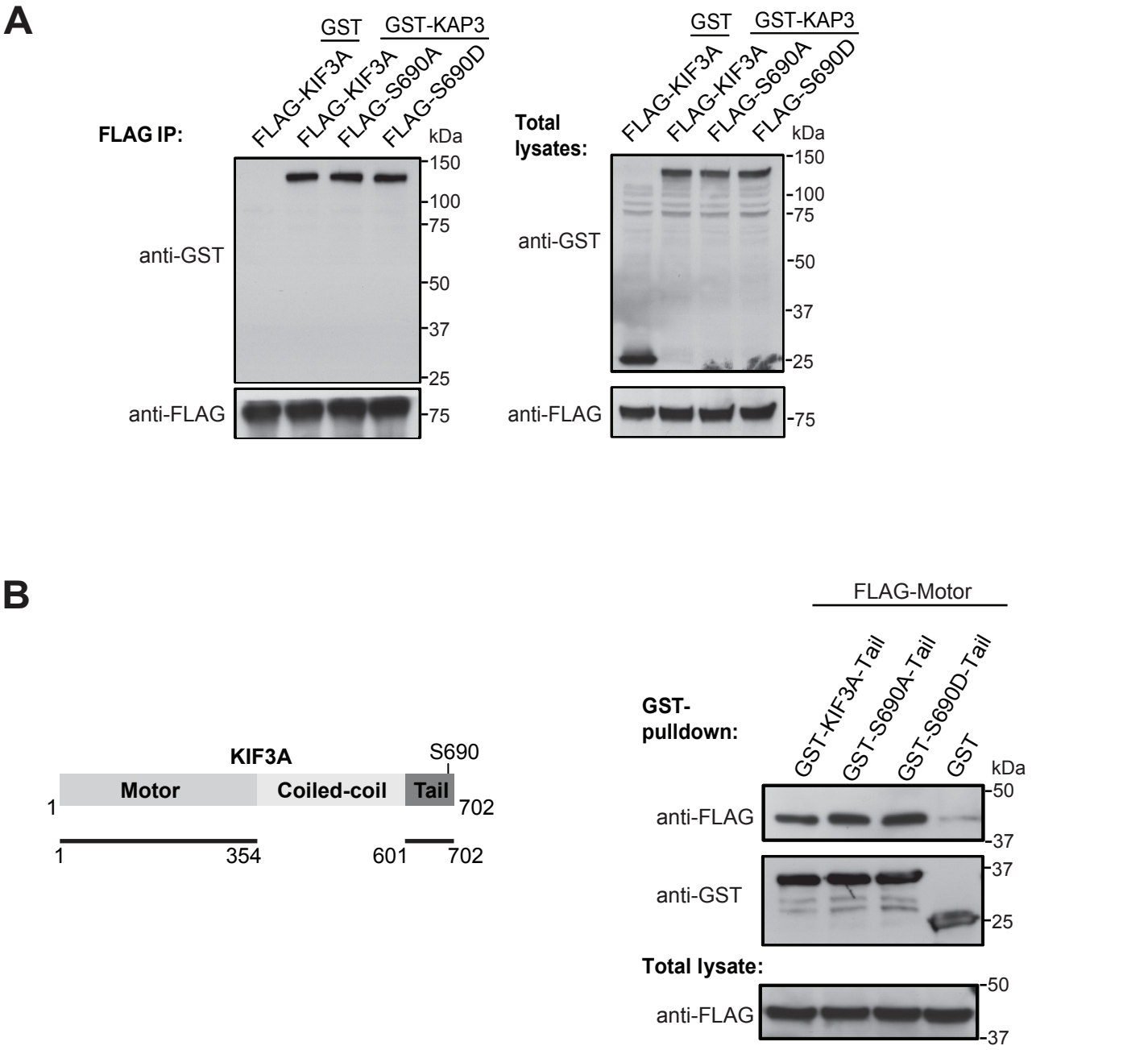
A
GST
GST-KAP3
FLAG-KIF3A
FLAG-KIF3A
FLAG-S690A
FLAG-S690D
FLAG IP:
kDa
150
100
75
50
37
25
anti-GST
anti-FLAG
75
Total lysates:
anti-GST
anti-FLAG
B
KIF3A
S690
Motor
Coiled-coil
Tail
1
702
1
354
601
702
FLAG-Motor
GST-KIF3A-Tail
GST-S690A-Tail
GST-S690D-Tail
GST
GST-pulldown:
anti-FLAG
anti-GST
Total lysate:
C
KIF3A
S690A
S690D
anti-FLAG
tubulin
input:
anti-FLAG
D
kDa
1
2
3
4
anti-phospho-Ser/Thr
FLAG-PAK1-P
FLAG-CaMKII-P
GST-KIF3A-Tail-P
anti- FLAG
Total FLAG-PAK1
Total FLAG-CaMKII
anti- GST
Total GST-KIF3A-Tail

Figure 6

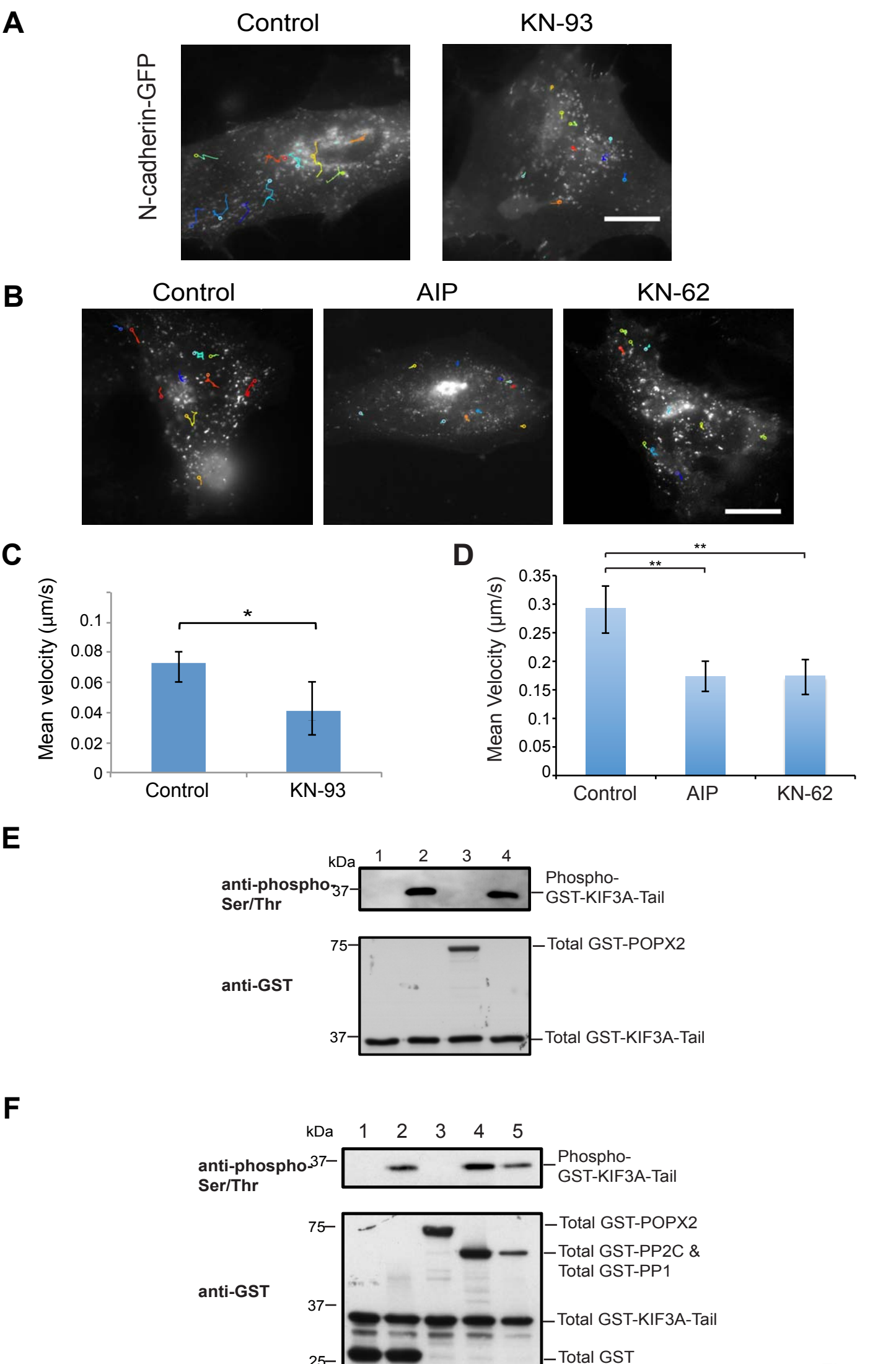
A
Control
KN-93
N-cadherin-GFP
B
Control
AIP
KN-62
C
Mean velocity (μm/s)
0.1
0.08
0.06
0.04
0.02
0
*
Control
KN-93
D
Mean Velocity (μm/s)
0.35
0.3
0.25
0.2
0.15
0.1
0.05
0
**
**
Control
AIP
KN-62
E
kDa
1
2
3
4
anti-phospho-Ser/Thr
37
Phospho-GST-KIF3A-Tail
75
Total GST-POPX2
anti-GST
37
Total GST-KIF3A-Tail
F
kDa
1
2
3
4
5
anti-phospho-Ser/Thr
37
Phospho-GST-KIF3A-Tail
75
Total GST-POPX2
Total GST-PP2C &
Total GST-PP1
anti-GST
37
Total GST-KIF3A-Tail
25
Total GST

Figure 7

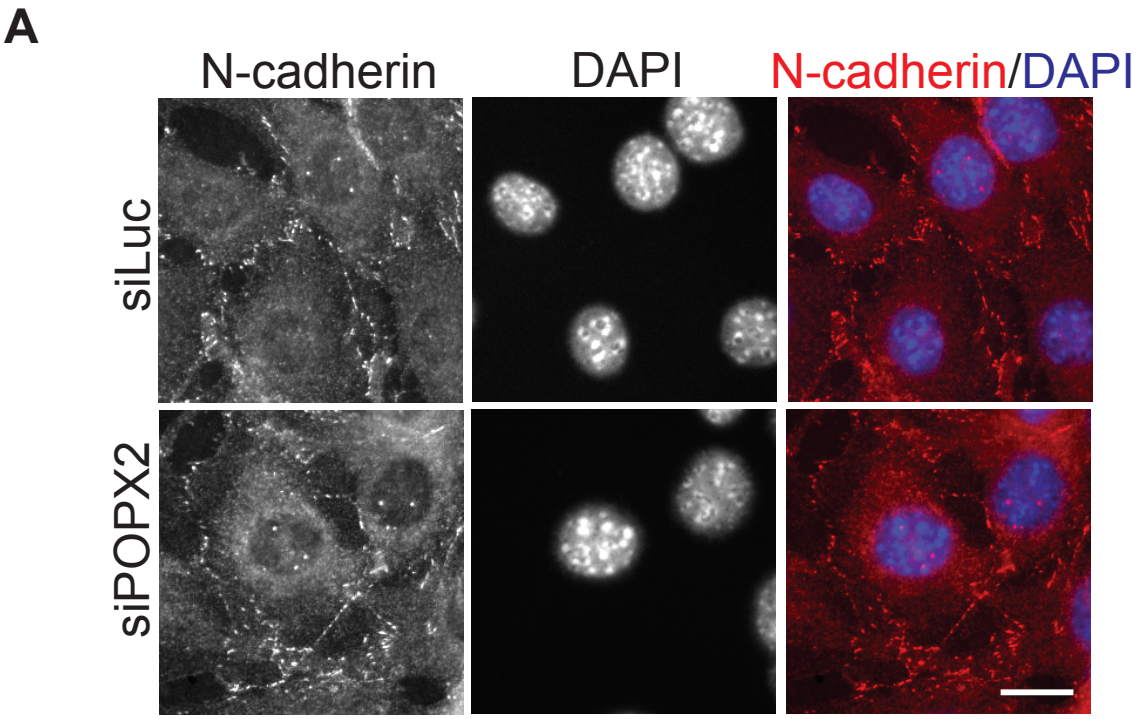
A
N-cadherin
DAPI
N-cadherin/DAPI
siLuc
siPOPX2

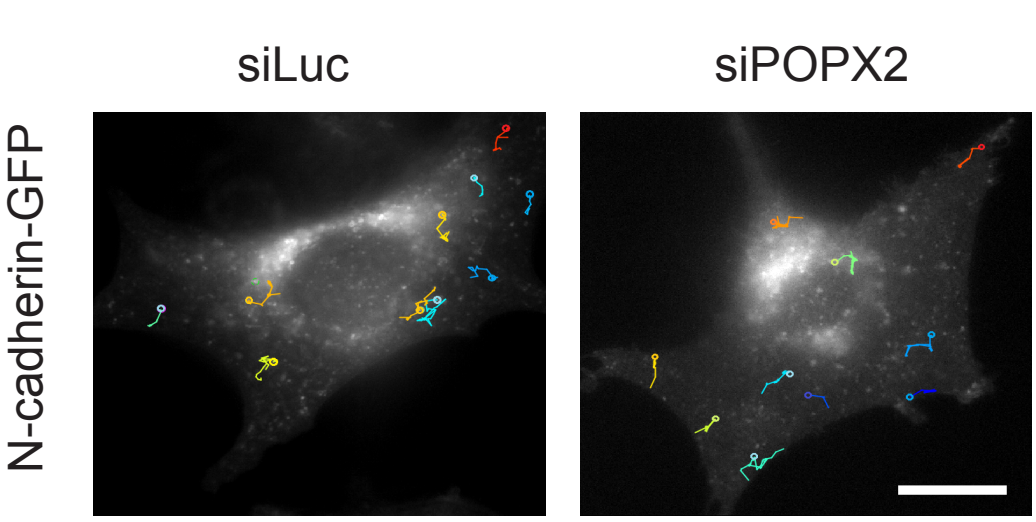
B
siLuc
siPOPX2
N-cadherin-GFP

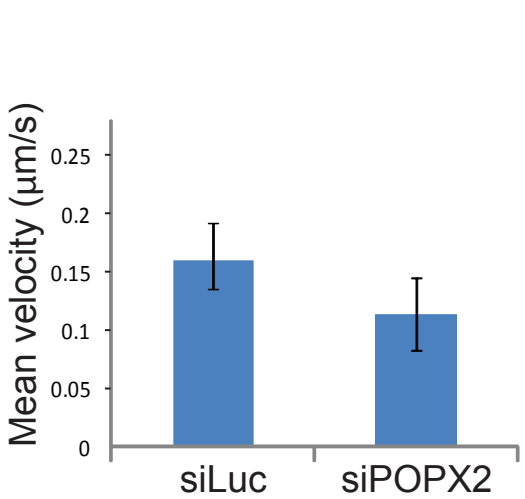
C
Mean velocity (µm/s)
0.25
0.2
0.15
0.1
0.05
0
siLuc
siPOPX2

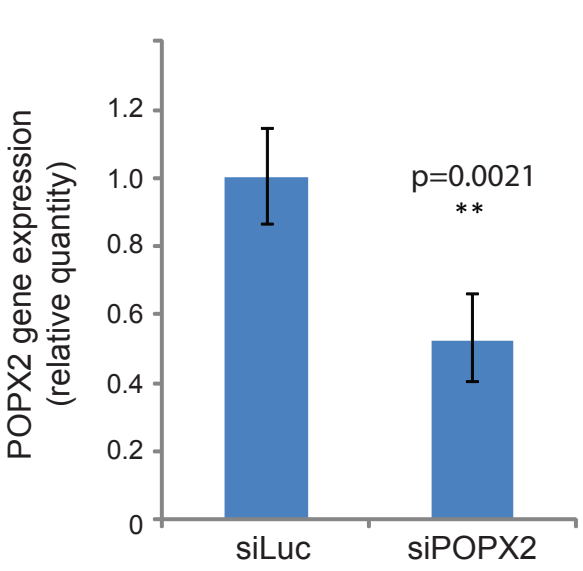
D
POPX2 gene expression
(relative quantity)
1.2
1.0
0.8
0.6
0.4
0.2
0
p=0.0021
**
siLuc
siPOPX2

Figure 8